In Situ Crosslinking of Poly(vinyl alcohol)/Graphene Oxide-Polyethylene Glycol Nano-composite Hydrogels as Artificial Cartilage Replacement: Intercalation Structure, Unconfined Compressive Behavior and Bio-tribological Behaviors

Yeqiao Meng [a], Lin Ye [a, *], Phil Coates [b], Peter Twigg [b]

[a] State Key Laboratory of Polymer Materials Engineering, Polymer Research Institute of Sichuan University, Chengdu, China

[b] School of Engineering, Faculty of Engineering and Informatics, University of Bradford, Bradford, UK

*: Corresponding author: Lin Ye

Address: State Key Laboratory of Polymer Materials Engineering

Polymer Research Institute of Sichuan University, Chengdu 610065, China

E-mail: yelinwh@126.com

Tel: 86-28-85408802

Fax: 86-28-85402465

In Situ Crosslinking of Poly(vinyl alcohol)/Graphene Oxide-Polyethylene Glycol Nano-composite Hydrogels as Artificial Cartilage Replacement: Intercalation Structure, Unconfined Compressive Behavior and Bio-tribological Behaviors

Yeqiao Meng [a], Lin Ye [a, *], Phil Coates [b], Peter Twigg [b]

[a] State Key Laboratory of Polymer Materials Engineering, Polymer Research Institute of Sichuan University, Chengdu, China
[b] School of Engineering, Faculty of Engineering and Informatics, University of Bradford, Bradford, UK

Abstract: Poly(vinyl alcohol) (PVA)/graphene oxide (GO) nano-composite hydrogel as artificial cartilage replacement was prepared via freezing/thawing method by introducing polyethylene glycol (PEG). Efficient grafting of PVA molecules onto GO surface was realized by formation of hydrogen bonding, resulting in exfoliation and uniform distribution of GO in PVA matrix. By introduction of appropriate content of GO, the increased crystalline regions of PVA and the formation of GO centered second network structure led to the increase of the storage modulus and effective crosslinking density. And therefore the mechanical strength and toughness of the composite hydrogel were improved simultaneously: the tensile strength, elongation at break and compressive modulus showed approximate 200%, 40% and 100% increase of the neat PVA hydrogel. Besides, for the sample with 1.5wt% GO content, the maximum force retention and dynamic stiffness were improved remarkably in the process of sinusoidal cyclic compression, and the compressive relaxation stress also increased significantly, indicating the enhancement of the compressive recoverable and anti-fatigue ability, and resistance to compressive relaxation by formation of high load-bearing, dense and reinforcing double network structure. Moreover, more than 50% decrease in coefficient of friction was obtained for the composite hydrogel, and the worn surface presented relative smooth and flat features with sharp decreasing furrow depth, confirming the lubrication effect of GO-PEG. This study shows promising potentials in developing new materials for cartilage replacement with simultaneous combination of high

mechanical property and excellent lubrication.

1. Introduction

Cartilage is a viscoelastic connective tissue consisting of relatively small numbers of cells covering the ends of long bones in diarthrodial joints, which provides one of the most efficient aqueous lubrication systems with the characteristic of simultaneous high load-bearing and low-friction property.[1-5] Unfortunately, due to the avascular nature and very limited capacity to repair, the articular cartilage is hard to heal once lesion or injury happens, causing cartilage replacement to be carried out in clinic.[6]

The materials for cartilage replacement need to sustain high loading, and comparable mechanical, lubricating properties and biocompatibility were required. Compared with the typical materials for artificial cartilage, like polyurethane (PU), poly(ether-ether-ketone) (PEEK), etc., poly(vinyl alcohol) (PVA) hydrogel has excellent biocompatibility, high mechanical property, high water absorption and low friction coefficient, thereby being recognized as a very promising substitute for cartilage repairing.[7-10] However, the PVA hydrogels normally exhibit inadequate strength and toughness for supporting the loads found in the joints, and inadequate sufficient lubrication. Therefore, the critical challenge in simultaneous combination of high mechanical property and excellent lubrication still exists.

Graphene is a two-dimensional planar sheet with one-atom-thickness of sp^2 carbon atoms arrayed in a hexagonal lattice.[11] Compared with other carbon fillers, such as graphite nanoplatelets (GNPs), it shows distinctive properties, like extremely high mechanical strength, superior electrical and thermal conductivity, excellent wear-resistant and self-lubricating property and high load-bearing capacity.[12-16] Especially, as an effective solid lubricant, graphene exhibits extraordinary self-lubricating and anti-wear properties ascribed to its easy shear ability and atomically smooth surface through

its intrinsic lamellar structure. Plenty of researches have been dedicated to the tribological behavior of graphene in both microscale and macroscale aspects, and proved graphene's capability in reducing wear rate.[17, 18] Graphene oxide (GO) is an important derivative of graphene with some oxygen functional groups on its surface, such as hydroxyl, epoxy, carboxyl, etc., which were easy to be designed and controlled to obtain the tailored interface by intermolecular linkage.[19-21] Moreover, GO was reported to show biocompatibility in recent researches.[22, 23] Lu Zhang fabricated the GO/PVA composite hydrogels with improved tensile strength (3.48MPa) and non-toxic effect on osteoblast cells.[24] Yifu Huang prepared boron-cross-linked GO/PVA hydrogel by freezing/thawing and boric acid crosslinking method, which showed tensile fracture strength (0.609 MPa) and high elongation rate (547%).[25] However, the mechanical strength of the reported PVA/GO hydrogels were far less than expected, and few literatures on dynamic mechanical and bio-tribological properties of the PVA/GO nanocomposite hydrogel can be available.

Polyethylene glycol (PEG) with flexible C-O-C chains showed superior self-lubricating property, and good compatibility simultaneously with both PVA and GO through hydrogen bonding.[26] Meanwhile, PEG is one of the most used biopolymers for the component of artificial cartilage.[27] In this work, the GO-PEG hybrid material was prepared by ultrasonic dispersion. Afterwards, due to the absence of any potential toxic additives, the freezing/thawing technics was chosen to prepare the PVA/GO-PEG nano-composite hydrogels.[28] The improvement of the compatibility between PVA and GO was expected to enhance both the mechanical and bio-tribological properties of PVA hydrogel, especially the dynamic compressive properties for simulating the compressive behaviors between bone joint and cartilage. The intercalation behavior and

structure, the network structure, the mechanical properties, dynamic compressive and bio-tribological behaviors of PVA/GO-PEG nano-composite hydrogels were studied.

2. Experimental

2.1 Materials

Poly(vinyl alcohol) (PVA) ($M_{n:}$ 74800 g/mol) was provided by Sichuan Vinylon Co. (China). Graphene oxide (GO) with a particle size of micron grade was provided by the Sixth Element Materials Technology Co. Ltd. (Changzhou, China). Polyethylene glycol (PEG) with an average molecular weight of 20000 was purchased from Kelong Chemical Reagents Co. Ltd. (Chengdu, China). Other chemical agents are all commercial grade products.

2.2 Preparation of PVA/GO-PEG nano-composite hydrogels

Firstly, a certain amount of GO was dispersed into 100 ml of deionized water under ultrasonication for 30 min at room temperature. Then PEG was added and the dispersion solution was sonicated at 70 ºC for another1 h. Afterwards 19.04 g PVA was added into the solution at 95 ºC with high speed stirring until being dissolved to obtain the PVA/GO-PEG dispersion solution. Then the solution was cooled to room temperature and poured into the mold, and the hydrogel films with 2 mm thickness and cylinders with 15 mm diameter were formed after 4 times of freezing at -20 ºC for 12 h and then thawing at room temperature for 4h.

2.3 Measurements

2.3.1 FTIR analysis

The structure of GO-PEG hybrid was analyzed with a Nicolet-560 Fourier-transform infrared spectrometer (FTIR) (U.S.A) under 20 min^{-1} of scanning rate and 4 $cm^{-1}$of resolution.[29]

2.3.2 Raman spectra analysis

The structure of GO-PEG hybrid was analyzed with Renishaw Invia Raman Microprobe (Britain) equipped with a 532 nm argon ion laser. Raman spectra were recorded from 1000 to 3500 cm^{-1}.

2.3.3 X-ray diffraction (XRD) analysis

XRD analysis of GO-PEG hybrid and dried PVA/GO-PEG nano-composite hydrogels was carried out with a Rigaku D/max ⅢB X-ray diffractometer (Japan) equipped with Cu Kα radiation (λ=0.154 nm) at an accelerating voltage of 40 kV and current of 40 mA. The d-spacing of samples were calculated with Bragg equation:[30]

$$2d\sin\theta = n\lambda \quad (1)$$

where θ is the diffraction angle; n is the order of diffraction and λ is the incident wavelength.

2.3.4 Transmission electron microscopy (TEM) analysis

TEM images of PVA/GO-PEG nano-composite hydrogel was observed on a JEOL JEM 100CX II TEM equipment (Japan) at an acceleration voltage of 200 KV. The samples were obtained by thin sections under cryogenic conditions and observed on 200-mesh copper grids.

2.3.5 Rheological property

The visco-elasticity property of PVA/GO-PEG nano-composite hydrogel were analyzed with Rheometer System Gemini 200 of Malvern Instrument Co. (UK) at 30 ^{o}C in the linear viscoelastic regime, while frequencies ranged from 0.1 to 100 Hz, at a maximum strain, γ of 0.1%.

2.3.6 Mechanical properties

The tensile properties of PVA/GO-PEG nano-composite hydrogel were measured with a 4302 material testing machine from Instron Co. (USA) according to ISO527/1-1993 (E). The samples in dumbbell shape with a size of 75×4×2 mm^3 were stretched

at a speed of 50 mm/min (23 ºC). Compressive strength and modulus of PVA/GO-PEG nano-composite hydrogels with the shape of cylinders of 8 mm (height) × 15 mm (diameter) were measured at a compression rate of 1mm/min.

2.3.8 Dynamic compressive behaviors

The sinusoidal cyclic compression and compressive stress-relaxation of PVA/GO-PEG nano-composite hydrogel samples were measured by using a Mach-1 Mechanical Test System (Biomomentum Inc, Canada). All the samples with the shape of cylinders of 8 mm (height) × 15 mm (diameter) were preloaded with 0.1 N to ensure contact. Sinusoidal cyclic compression were performed with an amplitude of 50% strain and frequency of 0.25 Hz for 50 cycles. For simulating the compression between bone joint and cartilage, the samples were compressed by a steel ball with a diameter of 5 mm and fixed in a room temperature PBS bath to keep hydrated. For the stress-relaxation test, the cylinder samples were deformed to 50% strain at a rate of 1mm/s and then allowed to relax for 300 s.

2.3.9 Friction and wear topography

Friction performance of PVA/GO-PEG nano-composite hydrogels were measured with a Universal Micro-Tribotester (UMT-2, CETR). In the test, the hydrogel samples with a size of 40 mm × 30 mm × 2 mm were fixed in a solution of normal saline (NS) or fetal bovine serum (FBS), respectively, and slid against a steel ball with a diameter of 10 mm. The weight load was 5 N and a relatively low shear rate of 60 mm/min^{-1} was set to avoid the hydrodynamic lubrication phenomenon.[31]

The morphologies of the worn surface of the samples at microscale were observed with a white-light interferometer (ContourGT-K 3D Optical Microscope, Germany) after the friction test. The samples were kept hydrated before the test.

3. Results and discussion

The GO-PEG hybrid was prepared by ultrasonic dispersion, and then PVA/GO-PEG nano-composite hydrogel was prepared through freezing/thawing technics, as shown in Figure 1.

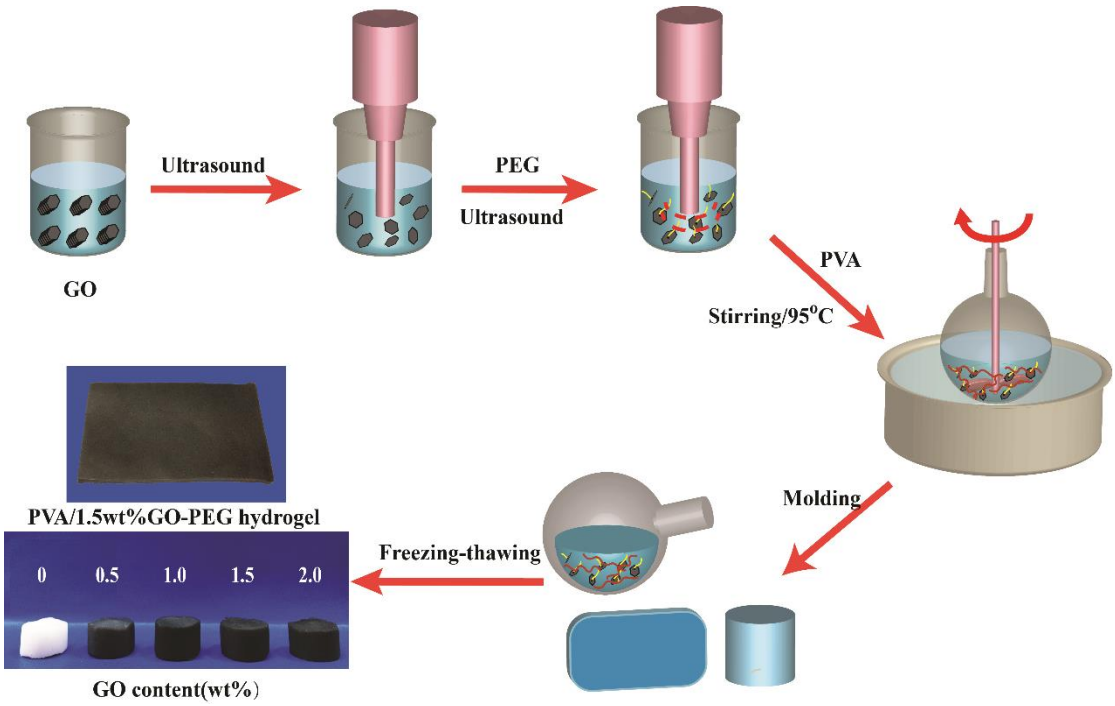

Figure 1. Preparation process of PVA/GO-PEG nano-composite hydrogel via freezing-thawing method

3.1 Intercalation structure of PVA/GO-PEG nano-composite

The PVA/GO-PEG dispersion solution was centrifugated and washed with hot distilled water to remove free PVA molecules. The obtained grafted GO sample was denoted as g-GO-PEG. For comparison, the grafted sample prepared in absence of PEG was denoted as g-GO. FTIR analysis of GO, g-GO and g-GO-PEG was shown in Figure 2a. For GO sample, the absorption peak at 3428 cm^{-1} was attributed to hydroxyl (-OH) stretching vibration. The absorption peaks at 1621 $cm^{-1}$and 1407 cm^{-1}corresponded to O-H bending vibration and CH-OH bending vibration, respectively. The absorption peaks at 1058 cm^{-1} and 856 cm^{-1} corresponded to C-O-C symmetric and asymmetric stretching vibration, respectively, while the absorption peak at 1230 cm^{-1} corresponded to C-O (alkoxy) stretching vibration.[32, 33] For g-GO, a slight red-shift of the absorption

peak attributed to O-H stretching vibration indicated hydrogen bonding for the composite system. For g-GO-PEG, some new absorption peaks appeared at 2921, 2857 and 1351 cm^{-1}, which could be attributed to the asymmetric, symmetric stretching and bending vibrations of methylene groups on PVA molecules. The peak at 1076 cm^{-1} was attributed to stretching vibration of C-O groups of PVA. Furthermore, the absorption peak corresponding to O-H stretching vibration had a further red-shift from 3428 cm^{-1} to 3409 cm^{-1} in comparison to GO, indicating the strong hydrogen bonding interaction for the composite system.

Figure 2b showed Raman spectra of GO, g-GO and g-GO-PEG. For GO sample, two absorption peaks at 1344.2 and 1583.6 cm^{-1} corresponded to the D band and G band, ascribing to structure defects and the first-order scattering of the E_{2g} vibration mode, respectively.[34, 35] For g-GO sample, besides the above D and G bands, no obvious absorption peak else appeared. For g-GO-PEG sample, the band around 2600-3000 cm^{-1} corresponding to the absorption peak of PVA molecules was observed, indicating that an abundance of PVA molecular chains was grafted onto GO layers. Moreover, for g-GO samples, the intensity ratio (I_D/I_G) presented a slight decrease from 0.98 to 0.91 in comparison to GO, while for g-GO-PEG sample, the I_D/I_G value deceased sharply to 0.84, indicating reduction of GO defect due to the anchoring effect of PEG and PVA molecules.[36] The schematic diagram of the hydrogen bonding interaction of composite system was shown in Figure 2c.

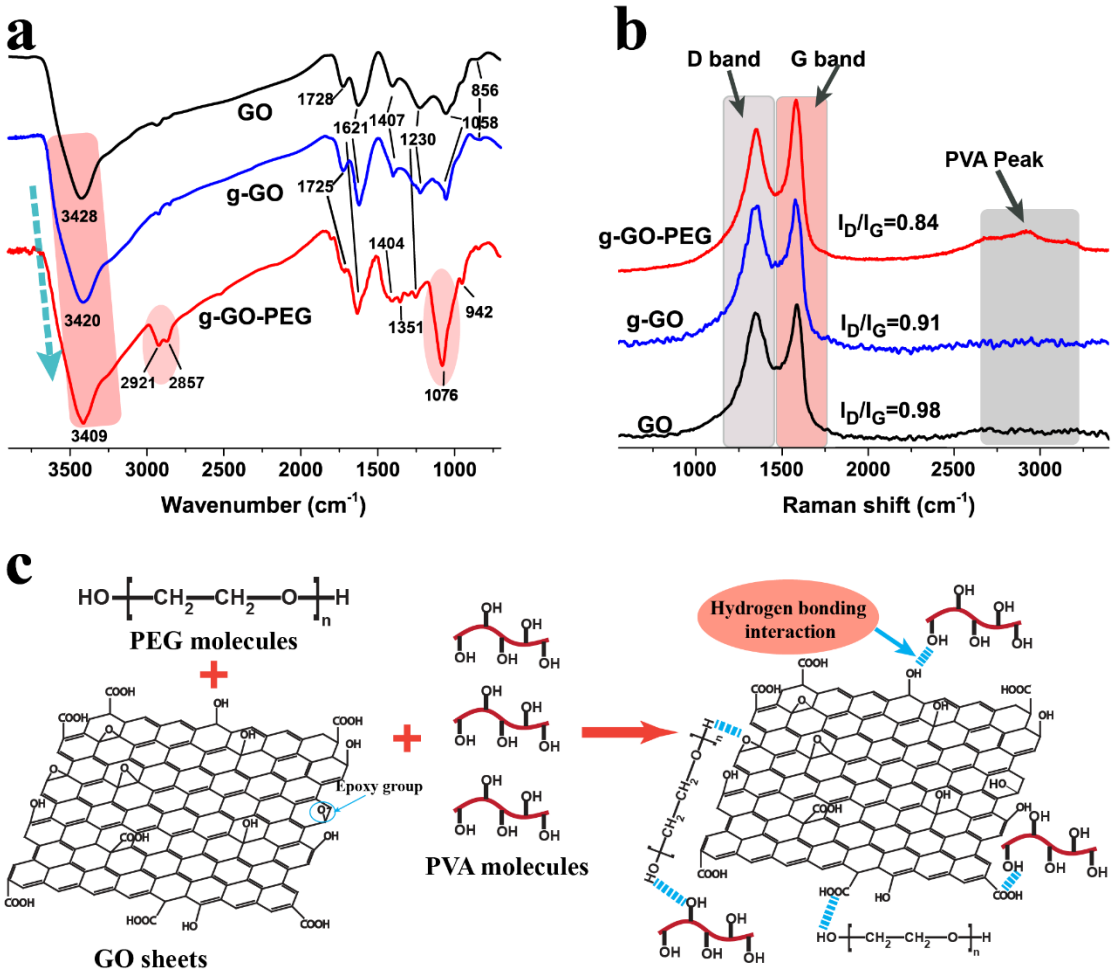

Figure 2. (a) FT-IR spectra and (b) Raman spectra of GO, g-GO and g-GO-PEG hybrids, (c) Anchoring effect of PEG and PVA molecules onto GO surface

The XRD patterns and characteristics of GO, g-GO and g-GO-PEG samples were shown in Figure 3a. The sharp peak for the (001) plane of GO was observed at 2θ=12.23°, corresponding to the interlayer spacing of ~0.7228 nm. For g-GO, the diffraction peak for the (001) plane shifted to lower angles (2θ = 10.70°), and the interlayer spacing increased to 0.8258, resulting from a few grafted PVA molecules on GO surface. For g-GO-PEG sample, the peak for the (001) plane disappeared, indicating the exfoliation and uniform distribution of GO in PVA matrix.[37] In addition, the new obvious diffraction peaks (2θ=19 °) corresponding to the crystalline form of PVA were observed, suggesting that more efficient grafting of PVA molecules onto GO surface was realized.

TEM micrographs of PVA/1wt% GO and PVA/1wt% GO-PEG nano-composite

hydrogels were shown in Figure 3b. GO in the PVA/1wt% GO sample showed a state of aggregation, while for the PVA/1wt% GO-PEG sample, GO was homogeneously distributed in PVA matrix (marked by arrows), demonstrating strong interfacial interaction and improved compatibility between GO and PVA molecules by introducing PEG.

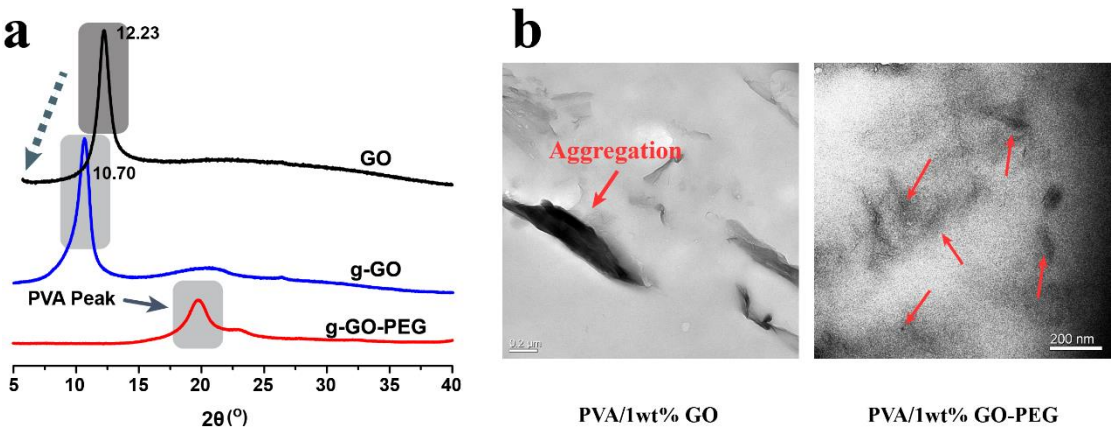

Figure 3. (a) XRD spectra of GO, g-GO and g-GO-PEG hybrids. (b) TEM images of PVA/1wt% GO and PVA/1wt%GO-PEG nano-composite hydrogel

3.2 The crystalline and crosslinking network structure of PVA/GO-PEG nano-composite hydrogel

During the freezing/thawing process, PVA molecules were frozen in the ice, and the van der Waals and hydrogen bonding force would promote the PVA molecules to form molecular entanglements and crystallites, which would act as crosslinking points in the physical crosslinking network.[38, 39] XRD diffraction analysis of the samples with different GO content were performed and shown in Figure 4a. The strong crystalline peaks in the 2θ range of 18~21° were the diffraction planes (101) of crystalline PVA. Meanwhile, with increasing GO content, the intensity of the diffraction planes (101) first increased and then decreased, reaching the maximum in presence of 1.5wt% GO.

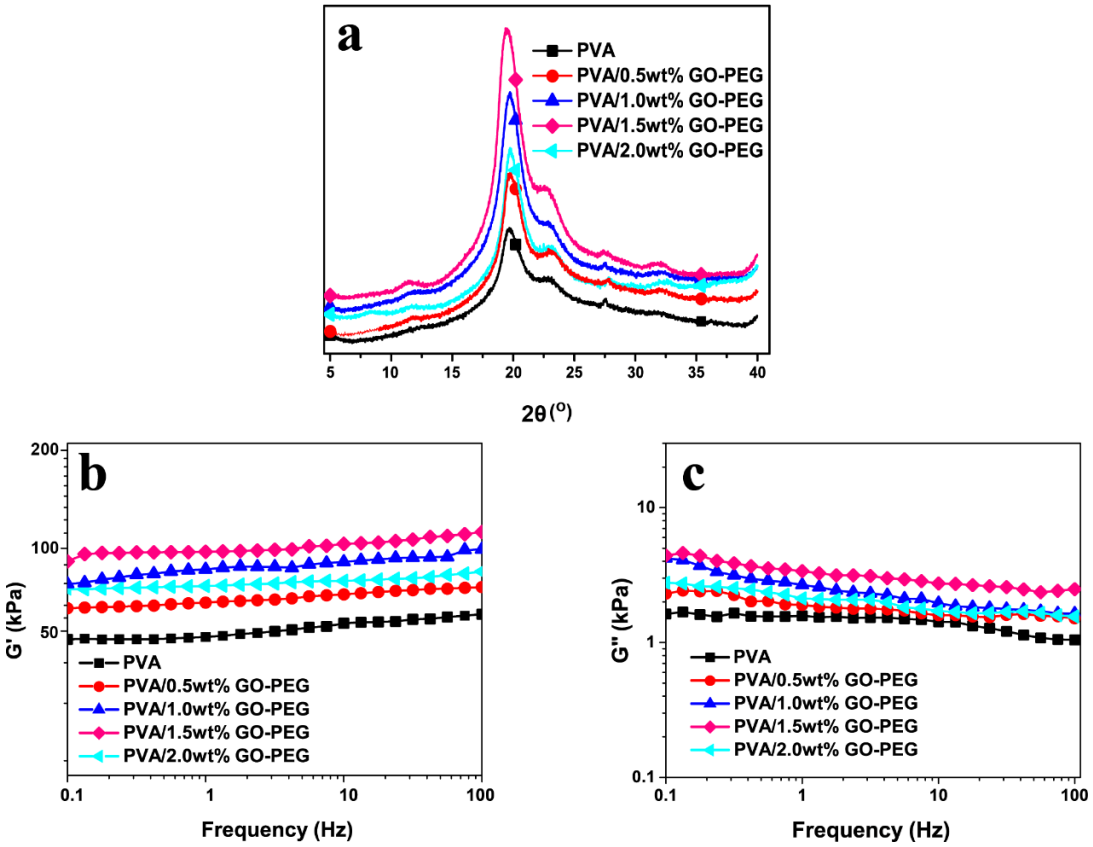

Figure 4. (a) XRD spectra of freezing dried PVA/GO-PEG nano-composite hydrogels with different GO content, (b) G' and (c) G" as a function of frequency for PVA/GO-PEG nano-composite hydrogels with different GO content

The crystallinity (X_c) of the PVA/GO-PEG nano-composite hydrogels was calculated from Figure 4a as the area ratio of the diffraction planes (101) to the whole diffraction of the sample.[40] As listed in Table 1, with increasing GO content, X_c first increased and then decreased, reaching the maximum in presence of 1.5wt% GO, more than 2-fold of the neat sample. This could be explained by that the GO sheets served as crystal nucleus to promote the crystal growth of PVA molecules in the process of network structure formation, while redundant GO sheets hindered the PVA molecules moving into the crystal lattice, resulting in the decrease of X_c.

Table 1. X_c of PVA/GO-PEG nano-composite hydrogels with different GO content

GO content (wt%)	2θ	X_c (%)
0	19.18	27.49
0.5	19.44	39.83

1	19.63	50.49
1.5	19.70	60.51
2	19.02	45.48

The frequency dependence of the shear storage modulus (G') and loss modulus (G") for PVA/GO-PEG nano-composite hydrogels were shown in Figure 4b and c. For all samples, G' was higher than G" and independent on the test frequency in the range of 0.1-100 Hz, indicating the existence of a network structure.[41] Meanwhile, with increasing GO content, G' increased first and then decreased, reaching the maximum in the presence of 1.5wt% GO.

The effective crosslinking density of the samples can be determined with the equation (2) based on the rubber elasticity theory:[42]

$$G' = RT\nu_e\varphi_2^{1/3}\varphi_1^{2/3} \quad (2)$$

where υ_e is the effective network density (mol/m^3), R is the gas constant (8.314 J/K•mol), T is the temperature (K). The volume fraction of the crosslinked polymer in the relaxed state (φ_1) and volume fraction of polymer in the hydrogel (φ_2) in swollen state can be calculated according to the reference,[42] and meanwhile, the average molecular mass (M_c) was calculated with the equation $M_c = \rho_p/\upsilon_e$, where ρ_p is the density of polymer.

The value of G', υ_e and M_c of the network were c listed in Table 2 for PVA/GO-PEG nano-composite hydrogels with various GO content. Obviously, G' and υ_e increased first, decreased afterwards, and reached the maximum in presence of 1.5wt% GO, at this point M_c reached the minimum, indicating that appropriate GO content could improve the crosslinking density of the nano-composite hydrogels. On one hand, introduction of GO could improve the crystallinity of PVA molecules which in company with PVA molecular entanglements could act as crosslinking points. On the other hand,

the hydrogen bonding interaction between GO sheets and PVA molecules led to the formation of the second network structure with GO as a crosslinking point by entanglement of PVA molecular chains grafted onto GO layers. However, excessive GO led to the aggregation of GO, resulting in the decrease of crystallinity of PVA molecules and υ_e.

Table 2. Network parameters of PVA/GO-PEG nano-composite hydrogels with different GO content

GO content (wt%)	ρ_p (g/cm^3)	φ_1	φ_2	G' (KPa)	ν_e (mol/m^3)	M_c (kg/mol)
0	1.24	1	0.15	53.32	40.68	30.38
0.5	1.24	1	0.16	68.03	50.68	24.37
1	1.24	1	0.16	85.96	63.82	19.35
1.5	1.24	1	0.17	97.38	72.00	17.15
2	1.24	1	0.17	76.50	56.68	21.79

3.3 Mechanical properties of PVA/GO-PEG nano-composite hydrogels

The tensile stress-strain curves of PVA/GO-PEG hydrogels with varying GO content were illustrated in Figure 5a and b. Obviously, the stress-strain curves for all samples presented an untypical stress yield behavior, and by incorporation of GO, compared with neat PVA hydrogel, PVA/GO-PEG hydrogels presented a sharp increase of the slope of linear portion of the stress-strain curves in the range of 60-100% strain (Figure 5b), indicating the orientation of GO sheets and PVA crystalline regions.

Figure 5c showed the tensile mechanical performances of PVA/GO-PEG hydrogels with varying GO content. The tensile strength and the elongation at break of the nano-composite hydrogels first increased, reaching the maximum at 1.5wt% GO content, and then decreased. Compared with neat PVA hydrogel, addition of 1.5wt% GO resulted in a roughly 200% increase in tensile strength, from 1.50 to 4.21 MPa, while the elongation at break increased by 40%. The significant reinforcement may be ascribed to the formation of a dense and stable crosslinking network with improved crystallinity

and υ_e. Besides, GO functionalized by PEG dispersed homogeneously in PVA matrix, resulting in the great achievement of excellent reinforcement effect of GO.

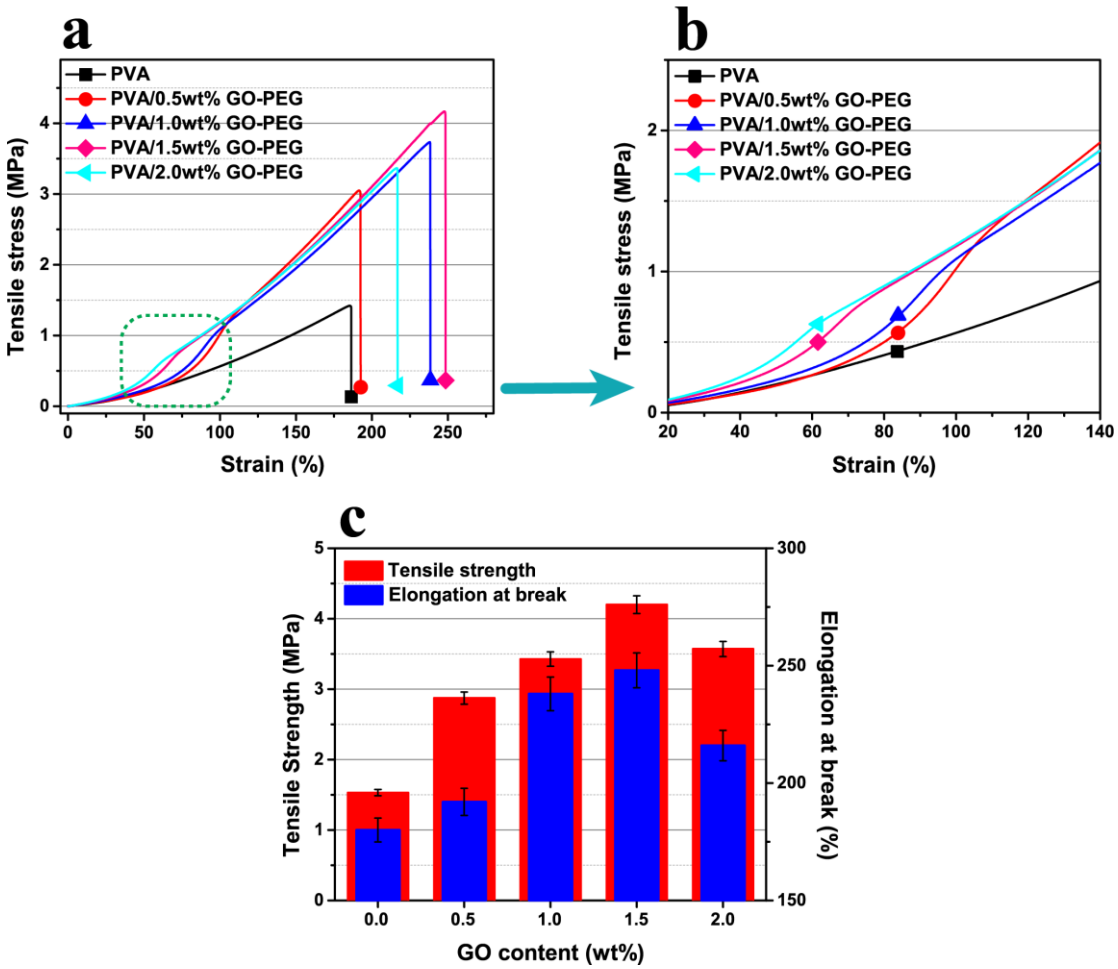

Figure 5. (a, b) Tensile stress-strain curves and (c) Mechanical properties of PVA/GO-PEG nano-composite hydrogels with different GO content

Unconfined compressive strength and compression modulus of PVA/GO-PEG nano-composite hydrogels with different GO content were illustrated in Figure 6a and b, respectively. The compression modulus was determined as the slope of linear portion of the stress-strain curves (10-15% strain).[43] The neat PVA hydrogels exhibited poor unconfined compressive modulus (0.54 MPa). With increasing GO content, the compressive strength and the compression modulus both showed the same trend of first increasing and then decreasing, reaching the maximum (1.12 MPa) at 1.5wt% GO content, more than 2-fold of the neat PVA hydrogel. Such high compression modulus was comparable with that of natural articular cartilage tissue (0.4-0.8 MPa).[44]

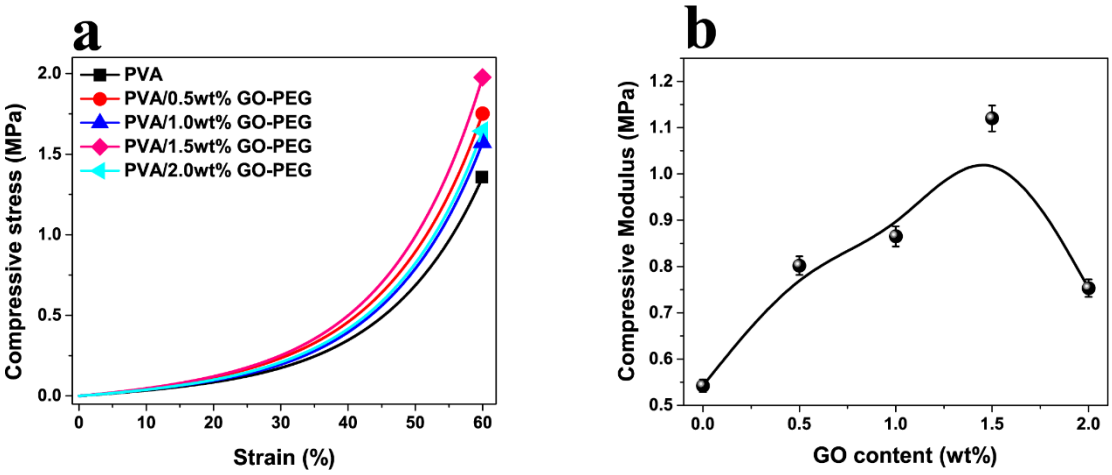

Figure 6. (a) Unconfined compressive stress-strain curves and (b) Compressive modulus of PVA/GO-PEG nano-composite hydrogels with different GO content

3.4 Dynamic and time-dependent compressive behaviors

The dynamic compressive behavior of PVA/GO-PEG hydrogels was performed by a sinusoidal cyclic compression, and indenter was in the shape of ball in order to simulate the compression between bone joint and cartilage (Figure 7a). Cyclic compression behavior of PVA/GO-PEG hydrogels was illustrated in Figure 7b. For all samples, with increasing cycle times, the maximum compressive force for each cycle first decreased rapidly and then gradually reached a balance. For further demonstrating the variation of the force, the maximum force retention rate (F_t/F_{max}) was defined as the ratio of the maximum force of each cycle (F_t) to the first cycle (F_{max}). Obviously, the plots of F_t/F_{max} for all samples exhibited three periods: in the initial stage, before about 5 cycle times, F_t/F_{max} declined sharply, indicating destruction of the delicate structure in the hydrogel. Afterwards, the F_t/F_{max} decreased slowly in the second stage and finally showed slight decrease in the third stage (after approximate 40 cycle times). After 50 cycles, F_t/F_{max} remained only 0.810 for the neat PVA hydrogel, while it increased up to 0.969 when the GO content was 1.5wt%, indicating the enhanced recoverable ability of the nano-composite hydrogels. The formation of the reinforcing double network structure helped to improve the anti-fatigue ability when being used in the process of

joint motion, such as jump and running.

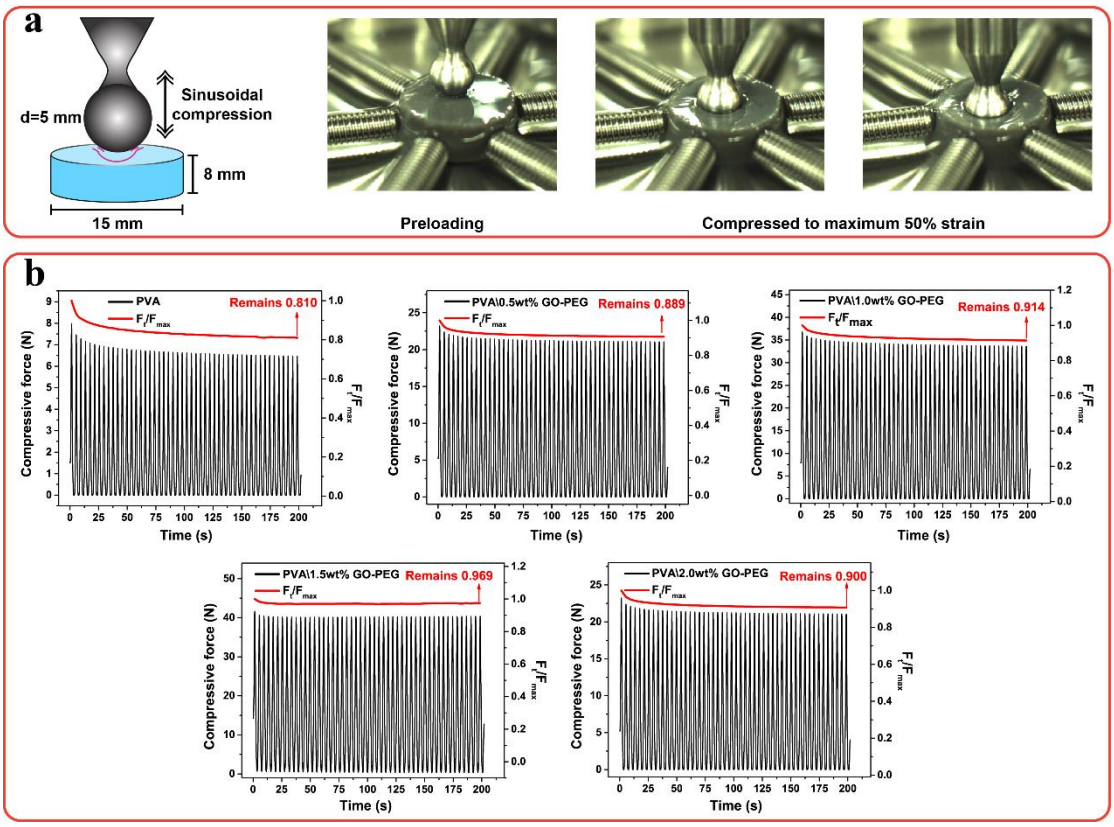

Figure 7. (a) Schematic illustration and photographs of the sinusoidal cyclic compression. (b) Compressive stress and F_t/F_{max} of PVA/GO-PEG nano-composite hydrogels as a function of time in response to a sinusoidal displacement in PBS

The dynamic stiffness was calculated as the ratio of the mean of maximum force of 45-50 cycles normalized by the amplitude of the applied displacement.[45] The dynamic stiffness of PVA/GO-PEG composite hydrogels was shown in Figure 8a. With the increase of GO content, the dynamic stiffness first increased and then decreased, reaching the maximum (8.1 N/mm) at 1.5wt% GO content, more than 4-fold increase of the neat PVA hydrogel (1.6 N/mm).

The phase angle (φ) was introduced for illustrating the lag between the sinusoidal strain and force[46] with the following equation:

$$\text{Phase angle} = (T_f\text{-}T_s)/T_0 \times 360 \quad (3)$$

where T_f and T_s were the time of force and strain reaching the maximum in the first cycles, respectively, and T_0 was the period of sinusoidal cycle (Figure 8b).

The phase angle of PVA/GO-PEG composite hydrogels in response to the first sinusoidal cycle were shown in Figure 8c. With the increase of GO content, the phase angle showed a trend of first increase and then decrease, reaching the minimum when GO content was 1.5wt%, which was consistent with the improving dynamic stiffness of the composite hydrogels.

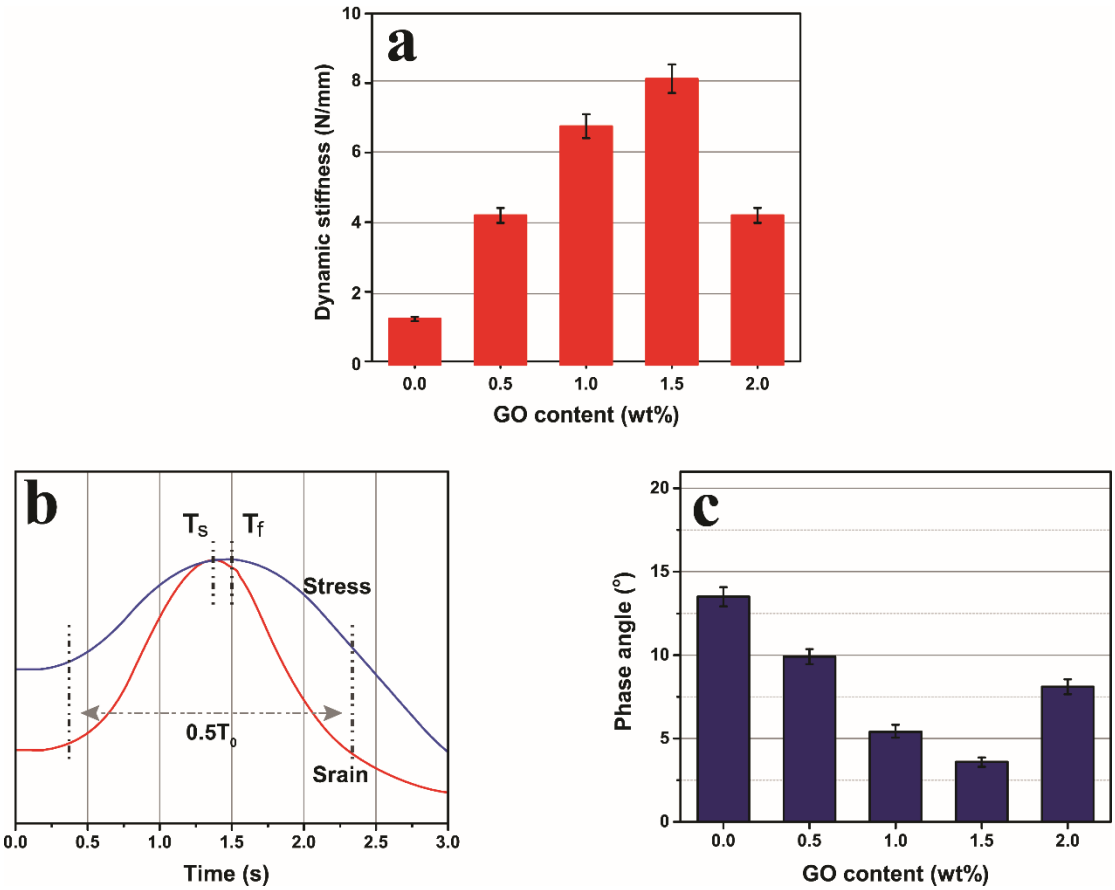

Figure 8. (a) Dynamic stiffness of PVA/GO-PEG nano-composite hydrogels with different GO content (b) Strain and stress curves of the neat PVA hydrogel in the first compressive cycle and (c) Phase angle of PVA/GO-PEG nano-composite hydrogels with different GO content

To compare the time-dependent mechanical properties of the PVA/GO-PEG nano-composite hydrogels with varying GO content, the stress-relaxation tests were performed (Figure 9a). For all samples, with increasing time, the compressive stress showed a trend of decrease at a different rate. Moreover, with the increase of GO content, the maximum compressive strength of the samples first increased and then decreased, reaching the maximum (1.08 MPa) at 1.5wt% GO content, more than 5-fold

increase of the neat PVA hydrogel (0.16 MPa).

The ratio of relaxation stress to the maximum stress (σ_t/σ_{max}) of PVA/GO-PEG nano-composite hydrogel as a function of time was shown in Figure 9b. Obviously, PVA/GO-PEG hydrogels exhibited much high σ_t/σ_{max}, especially for the sample with 1.5wt% GO content, σ_t/σ_{max} still remained 0.97 after 300s, more than 2-fold increase of the neat PVA hydrogel (0.31). For the neat PVA hydrogel, the crystalline regions and PVA molecular entanglements acted as the main crosslinking points of the network structure, which were easy to be destroyed during the long-time of being compressed. By introduction of GO, crystallinity of PVA increased and the network of the nano-composite hydrogels became denser, while the second GO centered network formed, which led to the achievement of the high load-bearing network with enhancement of resistance to network destruction and hindering the PVA molecules from relaxing during the compression.[47] As a result, the nano-composite hydrogels showed good time-dependent compressive ability when being used in the process of joint motion, such as long-time standing.

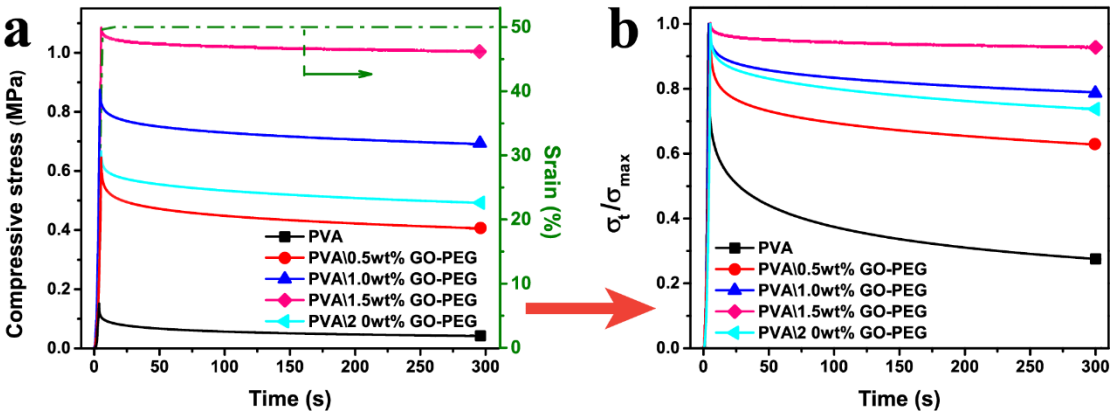

Figure 9. (a) Compressive stress-strain curves and (b) σ_t/σ_{max} of PVA/GO-PEG nano-composite hydrogels as a function of time in response to a compressive stress relaxation test

3.5 Bio-tribological behavior of PVA/GO-PEG nano-composite hydrogels

The coefficient of friction (COF) plots of PVA/GO-PEG nano-composite hydrogels as a function of time in normal saline (NS) and fetal bovine serum (FBS) were shown in Figure 10a and b, respectively. It can be seen that a time-dependent friction responses

were observed to be similar to real articular cartilage tissues.[48] At the beginning, all the samples showed very low COF which was related to the asperities and weak structure on the surface of the hydrogels.[5] Then, such structures were scraped and the surface became flat, accompanying with the gradual increasing and finally reaching a stable value of COF. With the increase of GO content, the equilibrium COF of the hydrogels first decreased and then increased, reaching a minimum in the presence of 1.5wt% GO, more than 50% decrease of the neat PVA hydrogel. Moreover, the COF plots in FBS showed a much slow increase and reached a lower equilibrium value in comparison with that in NS, resulting from the lubricating effect of FBS.

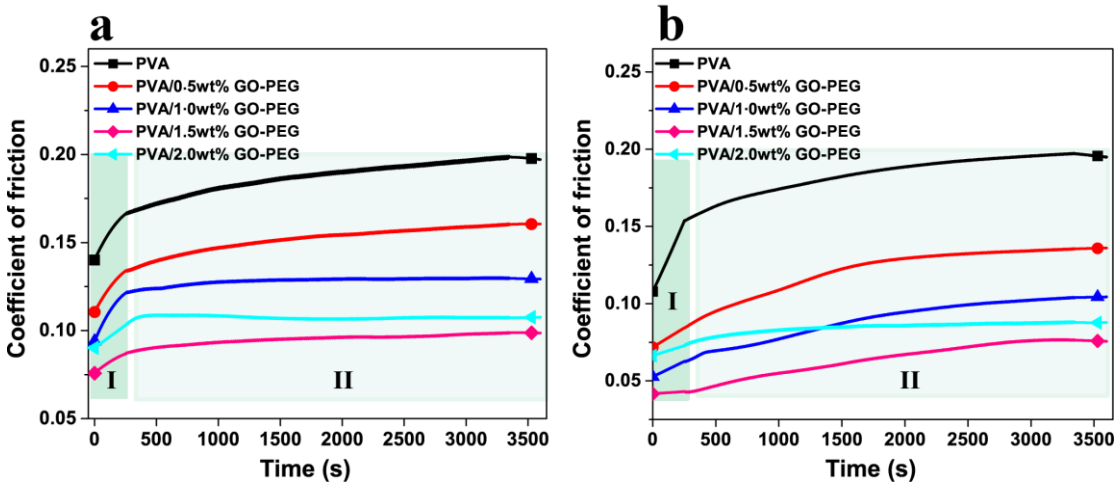

Figure 10. COF plots of PVA/GO-PEG nano-composite hydrogels as a function of time in (a) NS and (b) FBS

The optical photography and 3D surface morphologies of worn surfaces of samples with varying GO content were shown in Figure 11a-e and a'-e', respectively. By direct observation, obvious furrows could be seen on the surfaces of neat PVA hydrogel and the sample with the presence of 0.5wt% GO content (Figure 11a and b, marked with red arrows). In contrast, with the increase of GO content, the worn surface gradually presented relatively smooth and flat features, especially for the sample with 1.5wt% GO content (Figure 11d). However, with further increasing of GO, for the sample with 2.0wt% GO content, randomly distributed small pits appeared on the surface (Figure 11e).

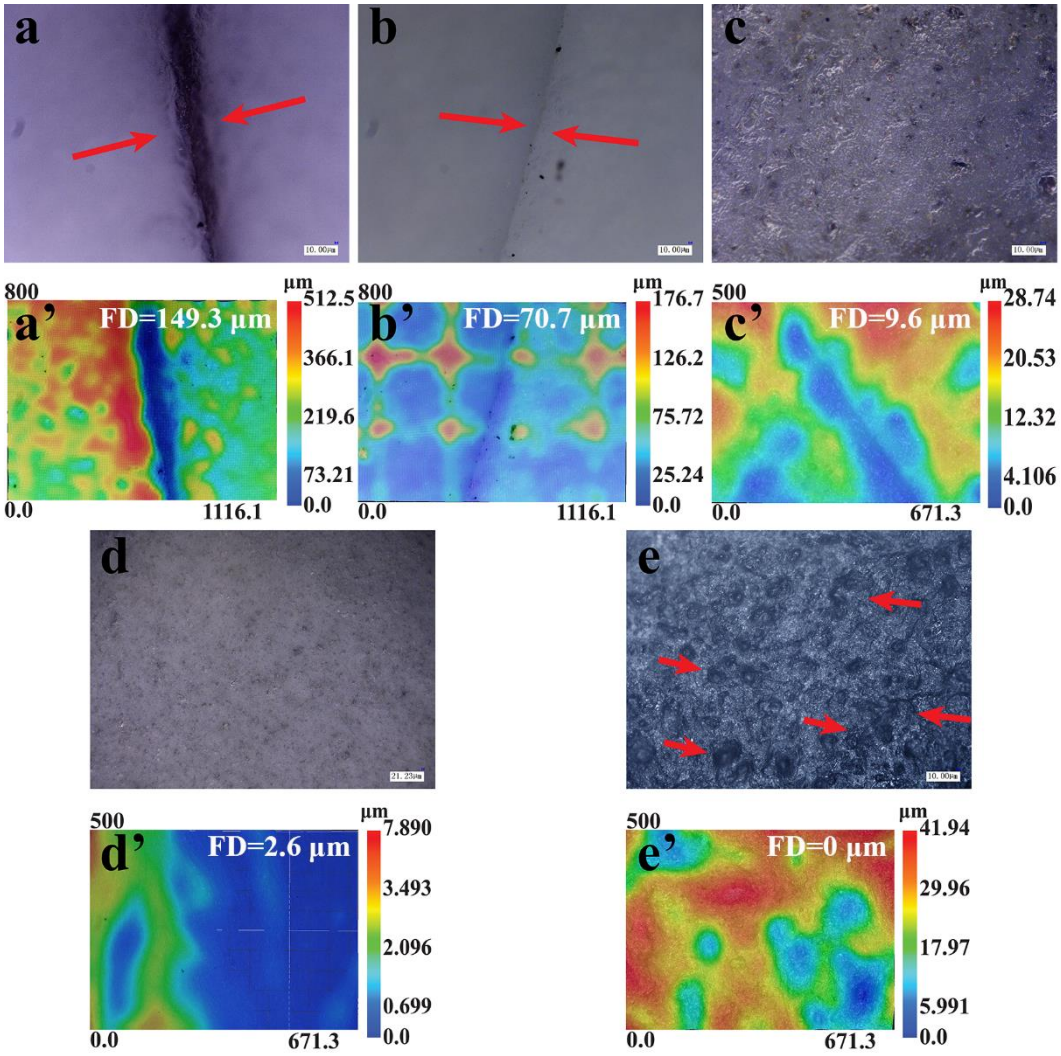

Figure 11. Optical photography, 3D surface morphologies and the furrow depth (FD) of worn surfaces of PVA/GO-PEG nano-composite hydrogels with varying GO content (a, a'-0, b, b'-0.5wt%, c, c'-1wt%, d, d'-1.5wt%, e, e'-2wt%)

3D surface morphologies showed a more visible change of the worn surface of the samples and the corresponding depth of the furrows distribution. As can be seen in Figure 11a', the neat PVA hydrogel exhibited relatively rough worn surface, with an approximate furrow depth (FD) of 149.3 μm. For PVA/0.5wt% GO-PEG sample, the furrow became significantly shallow and narrow, and the depth diminished rapidly to 70 μm (Figure 11b'). With further increase of GO content, for PVA/1.0wt% GO-PEG, the depth of furrow continued to decrease (Figure 11c, ~ 9.6 μm), and the furrow disappeared when the GO content reaching 1.5wt% (Figure 11d' and e'). The result demonstrated that during sliding, a protection layer formed on the sample surface to

resist deformation and the real contact area was reduced by compositing with GO-PEG. Moreover, GO provided low shear force, leading to homogenous depth distribution of the worn surface and low friction coefficient for the composite hydrogel. Meanwhile, PEG with self-lubricating property also helped to lower the friction coefficient. In addition, the improved mechanical strength of the composite was advantageous to the enhancement of its wear-resistance.[49]

4. Conclusions

A series of PVA/GO-PEG nano-composite hydrogels were prepared through freezing-thawing method. The result showed that introduction of PEG led to more efficient grafting of PVA molecules on GO surface, and GO was exfoliated and uniformly distributed in PVA matrix. By addition of appropriate content of GO, the crystallinity of the composite hydrogels increased dramatically, resulting from nucleation effect of GO sheets in the process of network structure formation. Meanwhile, the formation of GO centered second network structure by the hydrogen bonding interaction between GO sheets and PVA molecules led to a denser network structure with increased storage modulus and effective crosslinking density. Compared with neat PVA hydrogel, addition of only 1.5wt% content of GO led to a sharp increase of mechanical properties. Besides, the maximum force retention and dynamic stiffness showed a remarkable increase, and the compressive relaxation stress increased by 2-fold of the neat PVA hydrogel, indicating the enhancement of the compressive recoverable and anti-fatigue ability. The composite hydrogels presented a remarkably lower friction coefficient and much flatter worn surface, confirming the synergistic lubrication effect of GO-PEG.

Acknowledgement

This work was financially supported by State Key Laboratory of Polymer Materials Engineering of China（Grant No. sklpme2016-2-07）

References

(1) Camarero-Espinosa, S.; Rothen-Rutishauser, B.; Foster, E. J.; Weder, C. Articular cartilage: from formation to tissuie engineering. *Biomater. Sci-UK.* **2016,** *4*, 734-767.

(2) Xiao, H.; Kim, S.; He, X.; Zhou, D.; Li, C.; Liang, H. Friction pair evaluation of cartilage–diamond for partial joint repair. *Carbon* **2014,** *80*, 551-559.

(3) Kienle, S.; Boettcher, K.; Wiegleb, L.; Urban, J.; Burgkart, R.; Lieleg, O.; Hugel, T. Comparison of friction and wear of articular cartilage on different length scales. *J. Biomech.* **2015,** *48*, 3052-3058.

(4) Bas, O.; De-Juan-Pardo, E. M.; Meinert, C.; D'Angella, D.; Baldwin, J. G.; Bray, L. J.; Wellard, R. M.; Kollmannsberger, S.; Rank, E.; Werner, C.; Klein, T. J.; Catelas, I.; Hutmacher, D. W. Biofabricated soft network composites for cartilage tissue engineering. *Biofabrication* **2017,** *9*, 025014-025028.

(5) Morita, Y.; Tomita, N.; Aoki, H.; Sonobe, M.; Wakitani, S.; Tamada, Y.; Suguro, T.; Ikeuchi, K. Frictional properties of regenerated cartilage in vitro. *J. Biomech.* **2006,** *39*, 103-109.

(6) Schwartz, C. J.; Bahadur, S.; Mallapragada, S. K. Effect of crosslinking and Pt–Zr quasicrystal fillers on the mechanical properties and wear resistance of UHMWPE for use in artificial joints. *Wear* **2007,** *263*, 1072-1080.

(7) Gu, J. W.; Li, N.; Tian, L. D.; Lv, Z. Y.; Zhang, Q. Y., High Thermal Conductivity Graphite Nanoplatelet/Uhmwpe Nanocomposites. *RSC Adv.* **2015**, *5*, 36334-36339.

(8) Cao, Y.; Xiong, D.; Wang, K.; Niu, Y. Semi-degradable porous poly (vinyl alcohol) hydrogel scaffold for cartilage repair: Evaluation of the initial and cell-cultured tribological properties. *J. Mech. Behav. Biomed. Mater.* **2017,** *68*, 163-172.

(9) Grad, S.; Kupcsik, L.; Gorna, K.; Gogolewski, S.; Alini, M. The use of biodegradable polyurethane scaffolds for cartilage tissue engineering: potential and limitations. *Biomaterials* **2003,** *24*, 5163-5171.

(10) Wang, H.; Xu, M.; Zhang, W.; Kwok, D. T.; Jiang, J.; Wu, Z.; Chu, P. K. Mechanical and biological characteristics of diamond-like carbon coated poly aryl-ether-ether-ketone. *Biomaterials* **2010,** *31*, 8181-8187.

(11) Novoselov, K. S.; Geim, A. K.; Morozov, S. V.; Jiang, D.; Zhang, Y.; Dubonos, S. V.; Grigorieva, I. V.; Firsov, A. A. Electric Field Effect in Atomically Thin Carbon Films. *Science* **2004,** *306*, 666-669.

(12) Gu, J. W.; Liang, C. B.; Zhao, X. M.; Gan, B.; Qiu, H.; Guo, Y. Q.; Yang, X. T.; Zhang, Q. Y.; Wang, D. Y., Highly Thermally Conductive Flame-Retardant Epoxy Nanocomposites with Reduced Ignitability and Excellent Electrical Conductivities. *Compos. Sci. Technol.* **2017**, *139*, 83-89.

(13) Gu, J.; Lv, Z.; Yang, X.; Wang, G. e.; Zhang, Q., Fabrication and Properties of Thermally Conductive Epoxy Resin Nanocomposites Filled with Fgnps/Pnbrs Hybrid Fillers. *Sci. Adv. Mater.* **2016**, *8*, 972-979.

(14) Gu, J. W.; Du, J. J.; Dang, J.; Geng, W. C.; Hu, S. H.; Zhang, Q. Y., Thermal Conductivities, Mechanical and Thermal Properties of Graphite Nanoplatelets/Polyphenylene Sulfide Composites. *RSC Adv.* **2014**, *4*, 22101-22105.

(15) Lee, S. K.; Rana, K.; Ahn, J. H. Graphene Films for Flexible Organic and Energy Storage Devices. *J. Phys. Chem. Lett.* **2013,** *4*, 831-841.

(16) Huang, X.; Qi, X.; Boey, F.; Zhang, H. Graphene-based composites. *Chem. Soc. Rev.* **2012,** *41*, 666-686.

(17) Filleter, T.; Mcchesney, J. L.; Bostwick, A.; Rotenberg, E.; Emtsev, K. V.; Seyller, T.; Horn, K.; Bennewitz, R. Friction and dissipation in epitaxial graphene films. *Phys. Rev. Lett.* **2009,** *102*, 086102.

(18) Kim, K. S.; Lee, H. J.; Lee, C.; Lee, S. K.; Jang, H.; Ahn, J. H.; Kim, J. H.; Lee, H. J. Chemical Vapor Deposition-Grown Graphene: The Thinnest Solid Lubricant. *ACS nano* **2011,** *5*, 5107-5114.

(19) Liu, H.; Li, Y.; Wang, T.; Wang, Q. In situ synthesis and thermal, tribological properties of thermosetting polyimide/graphene oxide nanocomposites. *J. Mater. Sci.* **2012,** *47*, 1867-1874.

(20) Shen, J.; Yan, B.; Shi, M.; Ma, H.; Li, N.; Ye, M. One step hydrothermal synthesis of TiO2-reduced graphene oxide sheets. *J. Mater. Chem.* **2011,** *21*, 3415-3421.

(21) Fan, F.; Zhang, B.; Cao, Y.; Yang, X.; Gu, J.; Chen, Y., Conjugated Polymer Covalently Modified Graphene Oxide Quantum Dots for Ternary Electronic Memory Devices. *Nanoscale* **2017**, *9*, 10610-10618.

(22) Zang, Z.; Zeng, X.; Wang, M.; Hu, W.; Liu, C.; Tang, X. Tunable photoluminescence of water-soluble AgInZnS–graphene oxide (GO) nanocomposites and their application in-vivo bioimaging. *Sensor Actuat. B-Chem.* **2017,** *252*, 1179-1186.

(23) Modi, A.; Verma, S. K.; Bellare, J. Graphene oxide nanosheets and d-alpha-Tocopheryl polyethylene glycol 1000 succinate (TPGS) doping improves biocompatibility and ultrafiltration in polyethersulfone hollow fiber membranes. *J. Colloid Interf. Sci.* **2017,** *504*, 86-100.

(24) Zhang, L.; Wang, Z.; Xu, C.; Li, Y.; Gao, J.; Wang, W.; Liu, Y. High strength graphene oxide/polyvinyl alcohol composite hydrogels. *J. Mater. Chem.* **2011,** *21*, 10399-10406.

(25) Huang, Y.; Zhang, M.; Ruan, W. High-water-content graphene oxide/polyvinyl alcohol hydrogel with excellent mechanical properties. *J. Mater. Chem. A* **2014,** *2*, 10508-10515.

(26) Zhang, S.; Xiong, P.; Yang, X.; Wang, X. Novel PEG functionalized graphene nanosheets: enhancement of dispersibility and thermal stability. *Nanoscale* **2011,** *3*, 2169-2174.

(27) Wang, J.; Zhang, F.; Tsang, W. P.; Wan, C.; Wu, C. Fabrication of injectable high strength hydrogel based on 4-arm star PEG for cartilage tissue engineering. *Biomaterials* **2017,** *120*, 11-21.

(28) Yamaoka, H.; Asato, H.; Ogasawara, T.; Nishizawa, S.; Takahashi, T.; Nakatsuka, T.; Koshima, I.; Nakamura, K.; Kawaguchi, H.; Chung, U. I.; Takato, T.; Hoshi, K. Cartilage tissue engineering using human auricular chondrocytes embedded in different hydrogel materials. *J. Biomed. Mater. Res. A* **2006,** *78*, 1-11.

(29) Gu, J. W.; Yang, X. T.; Lv, Z. Y.; Li, N.; Liang, C. B.; Zhang, Q. Y., Functionalized Graphite Nanoplatelets/Epoxy Resin Nanocomposites with High Thermal Conductivity.

Int. J. Heat Mass. Transf. **2016**, *92*, 15-22.

(30) Li, C.; Xiang, M.; Ye, L. Intercalation Behavior and Orientation Structure of Graphene Oxide/Polyethylene glycol Hybrid Material. *Rsc Adv.* **2016,** *6*, 72193-72200.

(31) Ateshian, G. A. The Role of Interstitial Fluid Pressurization in Articular Cartilage Lubrication. *J. Biomech.* **2009,** *42*, 1163-1176.

(32) Tan, P.; Wen, J. J.; Hu, Y. Y.; Tan, X. J. Adsorption of Cu^{2+} and Cd^{2+} from aqueous solution by novel electrospun poly(vinyl alcohol)/graphene oxide nanofibers. *Rsc Adv.* **2016,** *6*, 79641-79650.

(33) Szabó T.; Berkesi, O.; Forgó P.; Josepovits K.; Sanakis Y.; Petridis D.; I., D. Evolution of Surface Functional Groups in a Series of Progressively Oxidized Graphite Oxides. *Chem. Mater.* **2015,** *18*, 2740-2749.

(34) Ferrari, A. C.; Meyer, J. C.; Scardaci, V.; Casiraghi, C.; Lazzeri, M.; Mauri, F.; Piscanec, S.; Jiang, D.; Novoselov, K. S.; Roth, S.; Geim, A. K. Raman spectrum of graphene and graphene layers. *Phys. Rev. Lett.* **2006,** *97*, 187401-187404.

(35) Guo, J.; Ren, L. L.; Wang, R. Y.; Zhang, C.; Yang, Y.; Liu, T. X. Water dispersible graphene noncovalently functionalized with tryptophan and its poly(vinyl alcohol) nanocomposite. *Compos. Part B-Eng.* **2011,** *42*, 2130-2135.

(36) Paredes, J. I.; Villarrodil, S.; Solísfernández, P.; Martínezalonso, A.; Tascón, J. M. D. Atomic Force and Scanning Tunneling Microscopy Imaging of Graphene Nanosheets Derived from Graphite Oxide. *Langmuir* **2009,** *25*, 5957-5968.

(37) Cao, Y.; Feng, J.; Wu, P. Preparation of organically dispersible graphene nanosheet powders through a lyophilization method and their poly(lactic acid) composites.

Carbon **2010,** *48*, 3834-3839.

(38) Kumar, A.; Mishra, R.; Reinwald, Y.; Bhat, S. Cryogels: Freezing unveiled by thawing. *Mater. Today* **2010,** *13*, 42-44.

(39) Peppas, N. A. Turbidimetric studies of aqueous poly(vinyl alcohol) solutions. *Macromol. Chem. Phys.* **1975,** *176*, 3433–3440.

(40) Shi, Y.; Xiong, D.; Liu, Y.; Wang, N.; Zhao, X. Swelling, mechanical and friction properties of PVA/PVP hydrogels after swelling in osmotic pressure solution. *Mater. Sci. Eng. C Mater. Biol. Appl.* **2016,** *65*, 172-180.

(41) Meng, Y.; Ye, L. Synthesis and swelling property of superabsorbent starch grafted with acrylic acid/2-acrylamido-2-methyl-1-propanesulfonic acid. *J. Sci. Food Agr.* **2017,** *97*, 3831-3840.

(42) Meng, Y.; Ye, L. Synthesis and swelling property of the starch‐based macroporous superabsorbent. *J. Appl. Polym. Sci.* **2017,** *134*, 44855-44864.

(43) Chen, J.; Shi, X.; Ren, L.; Wang, Y. Graphene oxide/PVA inorganic/organic interpenetrating hydrogels with excellent mechanical properties and biocompatibility. *Carbon* **2016,** *111*, 18-27.

(44) Doulabi, A. H.; Mequanint, K.; Mohammadi, H. Blends and Nanocomposite Biomaterials for Articular Cartilage Tissue Engineering. *Materials* **2014,** *7*, 5327-5355.

(45) G. Vunjak‐Novakovic; I. Martin; B. Obradovic; S. Treppo; A. J. Grodzinsky; R. Langer; L. E. Freed. Bioreactor cultivation conditions modulate the composition and mechanical properties of tissue-engineered cartilage. *J. Orth. Res.* **2010,** *17*, 130-138.

(46) Lawless, B. M.; Sadeghi, H.; Temple, D. K.; Dhaliwal, H.; Espino, D. M.; Hukins, D. W. L. Viscoelasticity of articular cartilage: Analysing the effect of induced stress and the restraint of bone in a dynamic environment. *J. Mech. Behav. Biomed. Mater.* **2017,** *75*, 293-301.

(47) Soltz, M. A.; Ateshian, G. A. Experimental verification and theoretical prediction of cartilage interstitial fluid pressurization at an impermeable contact interface in confined compression. *J. Biomech.* **1998,** *31*, 927-934.

(48) Greene, G. W.; Israelachvili, J. N. Adaptive mechanically controlled lubrication mechanism found in articular joints. *P. Natl. Acad. Sci.* **2011,** *108*, 5255-5259.

(49) Li, C.; Xiang, M.; Ye, L. Intercalation Structure and Highly Enhancing Tribological Performance of Monomer Casting Nylon-6/Graphene Nano-composites. *Compos. Part a-Appl. S.* **2017,** *95*, 274-285.

Captions

Figure Captions

Figure 1. Preparation process of PVA/GO-PEG nano-composite hydrogel via freezing-thawing method

Figure 2. (a) FT-IR spectra and (b) Raman spectra of GO, g-GO and g-GO-PEG hybrids, (c) Anchoring effect of PEG and PVA molecules onto GO surface

Figure 3. (a) XRD spectra of GO, g-GO and g-GO-PEG hybrids. (b) TEM images of PVA/1wt% GO and PVA/1wt%GO-PEG nano-composite hydrogel.

Figure 4. (a) XRD spectra of freezing dried PVA/GO-PEG nano-composite hydrogels with different GO content, (b) G' and (c) G'' as a function of frequency for PVA/GO-PEG nano-composite hydrogels with different GO content.

Figure 5. (a, b) Tensile stress-strain curves and (c) Mechanical properties of PVA/GO-PEG nano-composite hydrogels with different GO content.

Figure 6. (a) Unconfined compressive stress-strain curves and (b) Compressive modulus of PVA/GO-PEG nano-composite hydrogels with different GO content

Figure 7. (a) Schematic illustration and photographs of the sinusoidal cyclic compression. (b) Compressive stress and F_t/F_{max} of PVA/GO-PEG nano-composite hydrogels as a function of time in response to a sinusoidal displacement in PBS

Figure 8. (a) Dynamic stiffness of PVA/GO-PEG nano-composite hydrogels with different GO content, (b) Strain and stress curves of the neat PVA hydrogel in the first compressive cycle and (c) Phase angle of PVA/GO-PEG nano-composite hydrogels with different GO content

Figure 9. (a) Compressive stress-strain curves and (b) σ_t/σ_{max} of PVA/GO-PEG nano-composite hydrogels as a function of time in response to a compressive stress relaxation test

Figure 10. COF plots of PVA/GO-PEG nano-composite hydrogels as a function of time in (a) NS and (b) FBS

Figure 11. Optical photography, 3D surface morphologies and the furrow depth (FD) of worn surfaces of PVA/GO-PEG nano-composite hydrogels with varying GO content (a, a'-0, b, b'-0.5wt%, c, c'-1wt%, d, d'-1.5wt%, e, e'-2wt%)

Table Captions

Table 1. X_c of PVA/GO-PEG nano-composite hydrogels with different GO content

Table 2. Network parameters of PVA/GO-PEG nano-composite hydrogels with different GO content

TOC Graphic

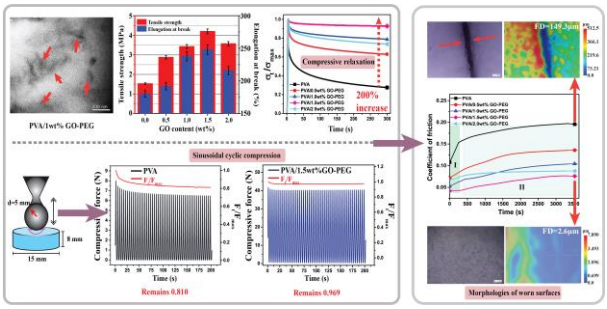
PVA/1wt% GO-PEG
Tensile strength
Elongation at break
Tensile strength (MPa)
Elongation at break (%)
GO content (wt%)
Compressive relaxation
200% increase
Time (s)
Sinusoidal cyclic compression
d=5 mm
8 mm
15 mm
PVA
PVA/1.5wt%GO-PEG
Compressive force (N)
Time (s)
Remains 0.810
Remains 0.969
Coefficient of friction
Morphologies of worn surfaces